Synthesis of Uniform Disk-Shaped Copper Telluride Nanocrystals and Cation Exchange to Cadmium Telluride Quantum Disks with Stable Red Emission – Supporting Information

Hongbo Li[1], *Rosaria Brescia*[1], *Mauro Povia*[1], *Mirko Prato*[1], *Giovanni Bertoni*[1,2], *Liberato Manna*[1] *and Iwan Moreels*[1,]*

[1] *Istituto Italiano di Tecnologia, via Morego 30, IT-16163 Genova, Italy.*

[2] *IMEM-CNR, Parco Area delle Scienze 37/A, IT-43124 Parma, Italy.*

* iwan.moreels@iit.it

Table S1. Summary of conditions involved in the syntheses of Cu_2Te nanodisks.

Sample	Thiol	Temperature	TOPTe	Shape
Figure1,2,3	$C_{12}SH$	175°C	10 wt %	Disks
Figure S1	$C_{12}SH$	180°C	10 wt %	Disks
Figure S3a	$C_{12}SH$	160°C	10 wt %	Dots
Figure S3b	$C_{12}SH$	200°C	10 wt %	Alloy dots
Figure S4a	C_8SH	180°C	10 wt %	Dots, Rods
Figure S4b	$C_{18}SH$	180°C	10 wt %	Small dots
Figure S5a	$C_{12}SH$	180°C	5 wt %	Dots
Figure S5b	$C_{12}SH$	180°C	15 wt %	Disks

Cu_2Te self-assembly and room-temperature XRD pattern

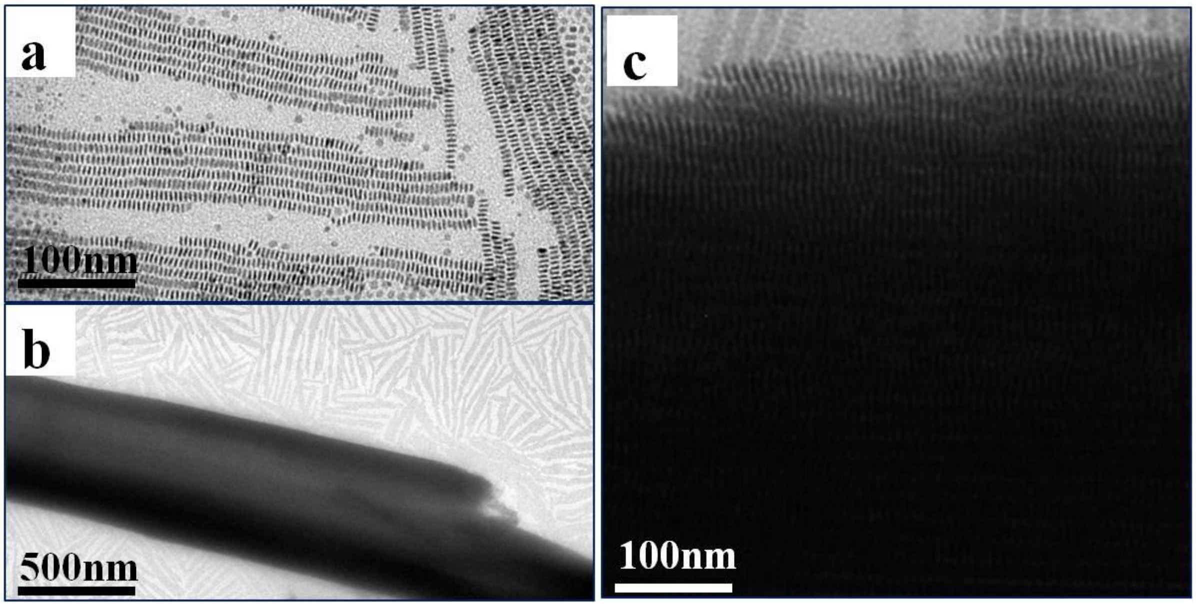

Figure S1: TEM images of the self assembly of Cu_2Te nanodisks, by adding acetonitrile as a nonsolvent according to previously reported procedures. (a) Nanoribbons of stacked Cu_2Te nanodisks. (b) Large-scale TEM image of attached nanoribbon strands. (c) Zoom of (b), showing the Cu_2Te nanodisk superlattice.

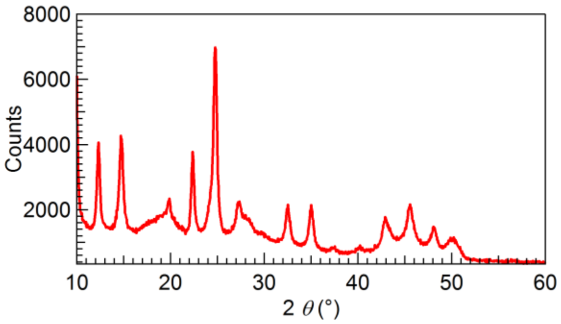

Figure S2: XRD pattern collected at room temperature for Cu2Te nanodisks. Several sharp reflections are observed, probably due to organic impurities. These are removed by annealing the sample in vacuum at 100 °C (see main text).

Cu_2Te synthesis conditions

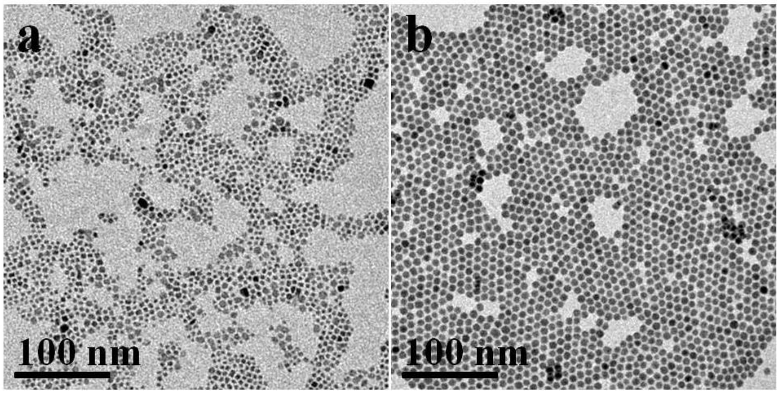

Figure S3: TEM images of Cu_2Te nanocrystals prepared at different temperature. (a) Injection of Te/TOP and growth of Cu_2Te at 160 °C leads to spherical nanocrystals of only 4.6 nm in diameter. (b) Raising the temperature only 20 °C above the typical reaction temperature of 180 °C, we again obtained spherical nanocrystals, here with a diameter of 7.4 nm.

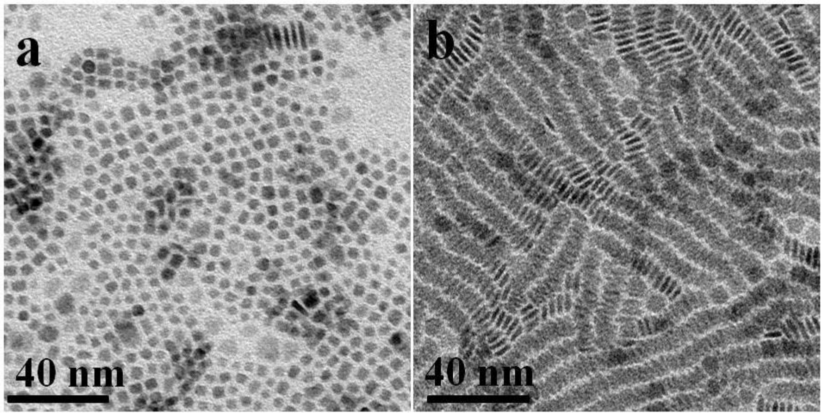

Figure S4: TEM images of Cu_2Te nanocrystals synthesized using TOPTe solutions with different concentrations, using the typical reaction temperature of 180 °C. (a) Reducing the Te concentration to 5 wt % produced polydisperse nanocrystals, with sizes ranging from 2 nm to 10 nm. (b) A Te concentration of 15 wt % gave uniform nanodisks, 12 nm in diameter.

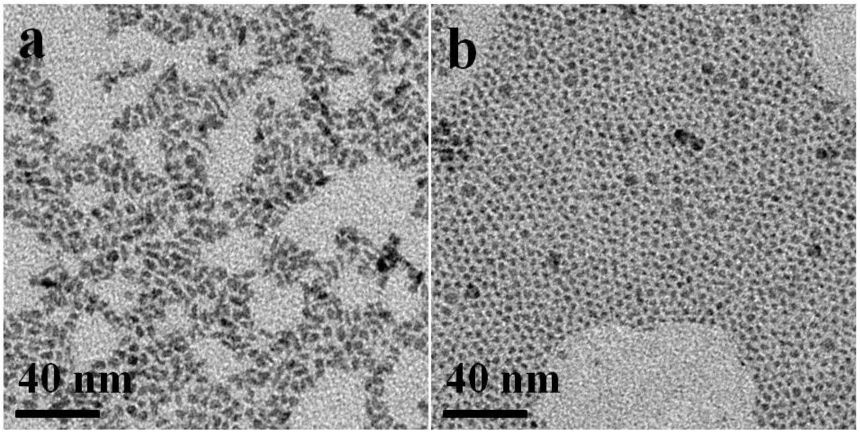

Figure S5: TEM images of Cu_2Te nanocrystals obtained by using thiols of different length. (a) 1-octanethiol (C_8SH) leads to a mixture of dots and short rods. (b) 1-octadecanethiol ($C_{18}SH$) results in dots around 2.5 nm in size, suggesting that the C_{18}-long chain length suppresses the nanocrystal growth.

CdTe high-temperature cation exchange

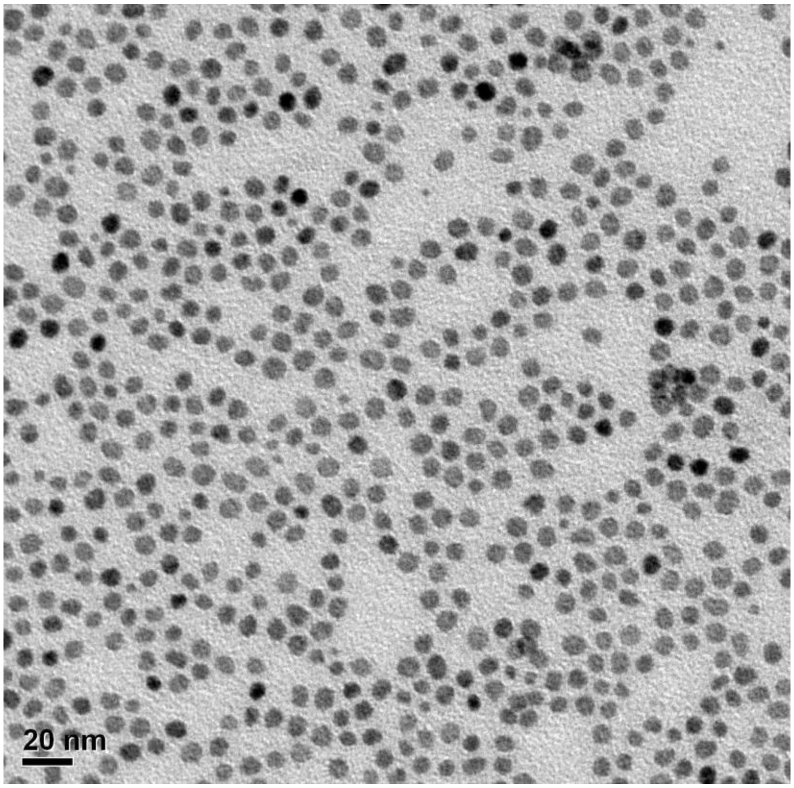

Figure S6: TEM images of the CdTe nanocrystals, obtained by performing the cation exchange reaction at 250 °C. The disks evolved into spherical quantum dots.

CdTe XRD pattern fitting

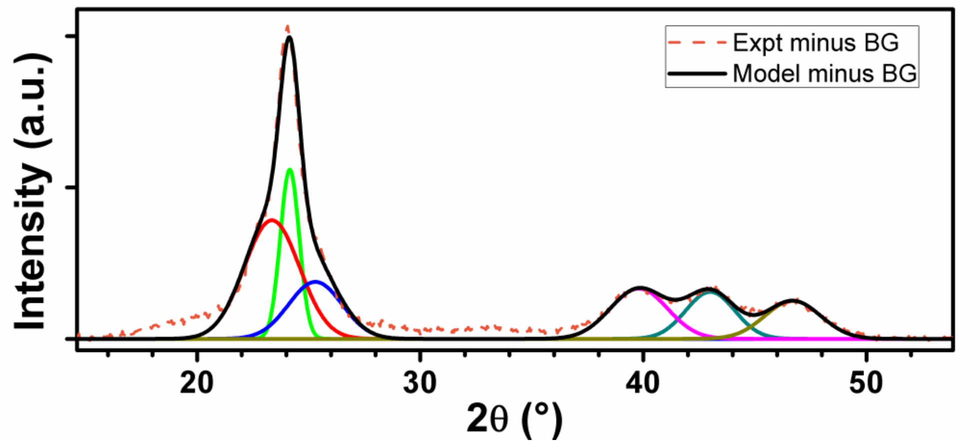

Miller indices	2θ (°)	d (Å)	size (nm)
002	24.15	3.68	8.1
101	25.30	3.52	2.9
100	23.35	3.81	2.8
103	43.0	2.10	3.3
110	39.8	2.26	2.8
112	46.7	1.94	2.9

Figure S7: Fit of the most intense peaks in the XRD pattern of CdTe using Gaussian functions, after subtraction of a linear background. The crystal size of the CdTe nanocrystals parallel to the respective lattice planes was calculated using the Scherrer equation $D = K\cdot\lambda/(\beta\cdot cos\theta)$. We took the instrumental broadening into account, evaluated by fitting the XRD pattern of a LaB_6 NIST standard collected under the same experimental conditions. The (002) peak is narrower than the others, giving a crystallite size of 8.1 nm which corresponds with the diameter obtained via HRTEM. The other peak values are in agreement with an average TEM size of 2.9±0.2 nm.

CdTe optical properties

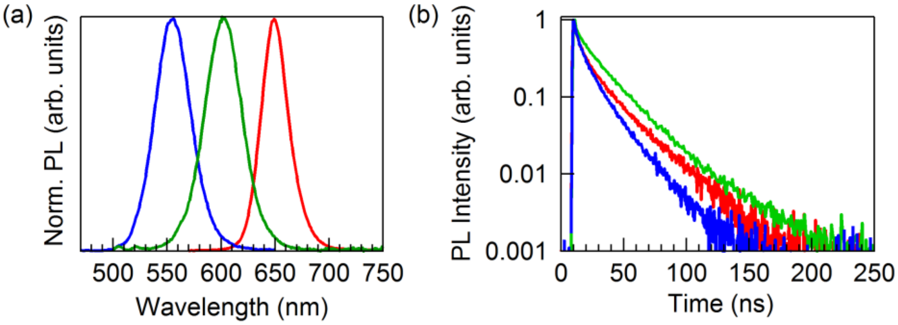

Figure S8: (a) PL spectra of 3.0 nm (blue), 3.5 nm (green) and 4.2 nm (red) spherical CdTe quantum dots. The full width at half maximum equals 24 nm, 25 nm and 19 nm, respectively. (b) Corresponding time-resolved PL decay traces.

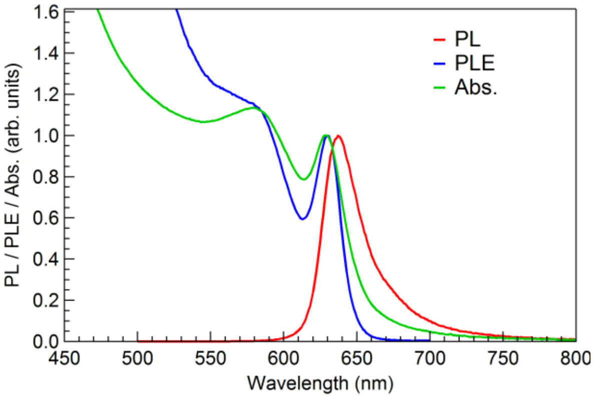

Figure S9: PL excitation spectrum for a CdTe quantum disk sample emitting at 637 nm. The PL is collected at the spectral position of the peak maximum, with an emission band width of 1 nm and an excitation band width of 3 nm. The resulting line width of the band-edge PLE peak is 22 nm, compared to 32 nm for the first absorption peak.

Table S2: Quantum disk thickness *h*, diameter *d*, and aspect ratio *AR* as derived from TEM measurements, and corresponding PL peak position. *As too few side-view images could be collected on the CdTe quantum disks, the Cu_2Te thickness is reported.

sample	*d* (nm)	*h* (nm)*	*AR*	PL peak (nm)
CdTe_2	6.77	2.30	2.94	621.7
CdTe_3	9.43	2.28	4.14	630.1
CdTe_5	9.99	2.38	4.20	636.6
CdTe_6	8.14	2.53	3.22	637.3
CdTe_7	8.16	2.11	3.87	603.0
CdTe_9	8.04	2.04	3.94	610.6

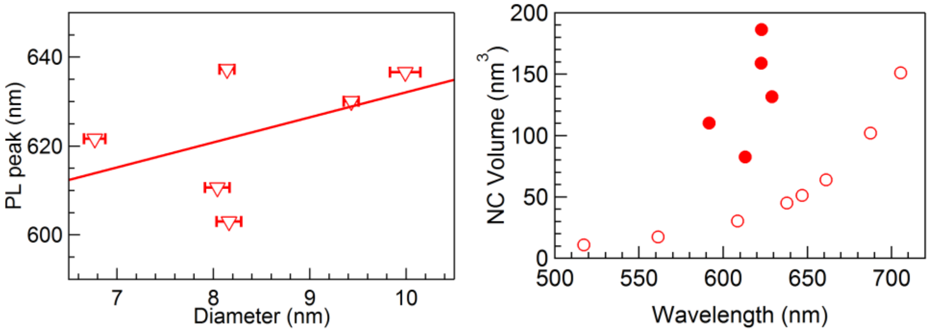

Figure S10: Left: Plot of the PL peak position as a function of the quantum disk diameter. In contrast with the thickness dependence (see main text), no clear blue shift with decreasing diameter is observed: the fitted line yields a slope of 5.6 ± 5.5. Right: Nanocrystal volume as a function of the spectral peak position of the first absorption peak for quantum dots (circles) and quantum disks (dots). The disks have a substantially larger volume for a given wavelength.

Sulfur XPS measurements

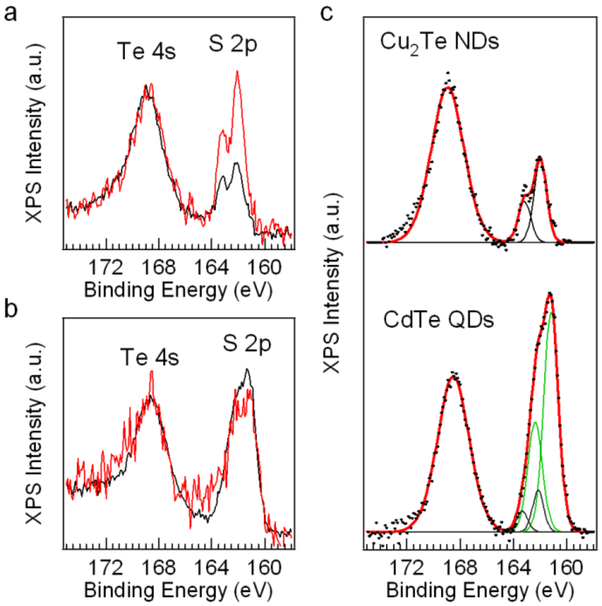

Figure S11: XPS characterization of Cu_2Te nanodisks (panel a) and CdTe quantum disks (panel b) as a function of the acquisition time (red curves: 10 minutes, black curves: 90 minutes). Data are shown in the energy region typical for Te 4s and S 2p peaks, after normalization of the intensity to the Te 4s peak. In the case of the Cu_2Te nanodisks, the S 2p peak intensity (and hence the amount of sulfur) decreased with time, while in the case of the CdTe quantum disks it remained constant. Panel c shows the deconvolution of S 2p peak of the Cu_2Te and CdTe disks respectively. Each S 2p doublet was identified by the position of the most intense $2p_{3/2}$ component. While in Cu_2Te the doublet (black) corresponds to the thiol ligands only, in CdTe we observed a second signal (green) that can be assigned to CdS. This suggests the formation of a monolayer of CdS on the CdTe surface.

Dielectric screening in quantum dots and disks

We calculated the average local field experienced in quantum dots and disks.[1] The latter were approximated by oblate spheres with an aspect ratio of 3.4:1, which equals the average value obtained from the quantum disks shown in figure 6c (taking the crystal reorganization after cation exchange into account). We obtained local field factors (*i.e.* the ratio of internal to external field) of $|f_{\mathrm{LF}}|^2 = 0.216$ and $|f_{\mathrm{LF}}|^2 = 0.308$ for dots and disks, respectively, using a refractive index of chloroform $n_{\mathrm{solv}} = 1.439$ and CdTe $n_{\mathrm{CdTe}} = 3.037$. We assume a negligible quantum disk extinction coefficient k near the band-edge in agreement with previous calculations on spherical nanocrystals.[2,3] Note that n_{CdTe} corresponds to the band-edge refractive index of zinc blende CdTe,[4] however, mixed zincblende/wurtzite CdTe thin films show similar refractive indices,[5] justifying the approach.

References

(1) Z. Hens, and I. Moreels, *J. Mater. Chem.* **2012**, *22*, 10406-10415.
(2) I. Moreels, K. Lambert, D. De Muynck, F. Vanhaecke, D. Poelman, J.C. Martins, G. Allan, and Z. Hens, *Chem. Mater.* **2007**, *19*, 6101-6106.
(3) I. Moreels, K. Lambert, D. Smeets, D. De Muynck, T. Nollet, J.C. Martins, F. Vanhaecke, A. Vantomme, C. Delerue, G. Allan, and Z. Hens, *ACS Nano* **2009**, *3*, 3023-3030.
(4) S. Adachi, T. Kimura, N. Suzuki, *J. Appl. Phys.* **1993**, *74*, 3435-3441.
(5) T.H. Myers, S.W. Edwards, J.F. Schetzina, *J. Appl. Phys.* **1981**, *52*, 4231-4237.